Thin-Skin Eddy-Current Interaction with Semielliptical and Epicyclic Cracks

J. R. Bowler, *Member, IEEE*, and N. Harfield

***Abstract*—Eddy-current probe impedance variations due to interactions with planar cracks have been calculated for the thin-skin regime. In this regime, the skin depth of the induced current is small compared to the crack depth and length, allowing approximations to be made. The approximations have been used by others to show that the thin-skin field at the surface of a crack is governed by a potential satisfying the two-dimensional (2–D) Laplace equation. In fact, the transverse magnetic potential at the crack face, defined with respect to the normal to this surface, satisfies a 2–D Laplace equation at an arbitrary skin depth. However, thin-skin boundary conditions applied at the crack perimeter greatly simplify the problem. Solutions of the Laplace problem for semielliptical cracks have been found by conformal mapping to a rectangular region. The surface potential in the rectangular domain is expressed as a Fourier series expansion and the coefficients of the series determined from the boundary conditions. Curved crack profiles of a general class, including semielliptic cracks as a special case, have been approximated by using ordered elliptical epicycles, a representation that retains the ability to map the crack domain to a rectangle. The probe impedance change due to a crack has been expressed in terms of the transverse magnetic potential and calculated from a line integral. Predictions of the probe impedance variations with position and frequency have been compared with an analytical solution for a semicircular crack and with experimental coil impedance measurements on semielliptical and epicyclic slots. Good agreement is observed in all comparisons.**

***Index Terms*—Crack, eddy current, nondestructive evaluation.**

I. Introduction

In EDDY-CURRENT nondestructive evaluation, cracks in metal components are detected through the changes in probe impedance that occur when induced current is perturbed. Testing for defects is commonly carried out at frequencies such that the electromagnetic skin depth is much smaller than the size of typical cracks. For example, the inspection of the interior of fastener holes on aircraft is carried out with the fasteners removed using a rotating probe operated at 500 kHz or more. At this frequency, the skin depth in an aluminum alloy structure is roughly 250 μm or less whereas the cracks are commonly a few millimeters long.

The thin-skin regime is of practical importance both for the inspection of nonferrous metals and for steels but it can be difficult to calculate high-frequency solutions. General three-dimensional numerical methods which use a nodal or mesh scheme to define a discrete approximation of the field are inefficient at small skin depths because a large number of unknowns may be required to achieve reasonable accuracy. This difficulty is avoided by adopting an approximation which allows the problem to be solved in terms of a surface potential satisfying the Laplace equation. The key to such an approach lies in finding the boundary conditions that apply to this potential at the mouth of the crack and at the buried edge.

A thin-skin eddy-current theory has been developed by Auld [1] for cracks in materials with the permeability of free space. Auld proposed an approximate boundary condition for the crack mouth which neglects the perturbed field due to the flaw. This approximation gives predictions that are in reasonable agreement with measurements in some cases [2], but comparisons with experimental results for a probe whose diameter is smaller than the crack depth reveals significant inaccuracies [3]. An alternative to Auld's approximation has been developed which takes into account the perturbed field at the crack mouth [4]. Although the new boundary condition is more complicated, it leads to improved predictions. Furthermore, it can be applied to materials of arbitrary permeability including ferromagnetic steels [3].

In this paper, eddy-current probe impedances due to semielliptical cracks in materials with a permeability of free space are calculated using accurate thin-skin boundary conditions. The present formulation uses a transverse magnetic potential to describe the interactions of the electromagnetic field with an idealized crack. Calculations for semielliptical cracks are performed by a conformal mapping to a rectangular region. This standard mapping has been generalized here to deal with a class of crack shapes that can be represented as elliptical epicycles. The representation uses a series expansion ordered according to the number of terms in the series, the semiellipse being the first-order case. Impedance predictions for elliptical and epicyclic cracks have been compared with experimental measurements performed on slots in aluminum plates. Further comparisons have been made with results derived from an analytical solution for a semicircular crack. These comparisons demonstrate the validity of the predictions.

Manuscript received February 28, 1999; revised August 3, 1999.

J. R. Bowler was with the Department of Physics, University of Surrey, Surrey, GU2 5XH U.K. He is now with the Electrical and Computer Engineering Department, Iowa State University, Ames, IA 50011 USA (e-mail: jbowler@cnde.iastate.edu).

N. Harfield is with the Center for Nondestructive Evaluation, Iowa State University, Ames, IA 50011-3042 USA.

Publisher Item Identifier S 0018-9464(00)00457-X.

II. Review of the Formulation

A. Scalar Decomposition

In the problem considered, eddy currents induced by a coil interact with a surface crack as shown in Fig. 1. The aim is to calculate a scalar potential representing the field at the crack

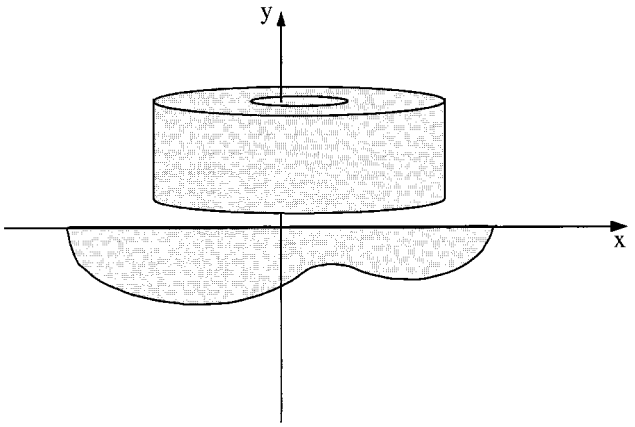

Fig. 1. A normal coil over a surface-breaking crack in a conductor.

surface and, from the solution, determine the coil impedance change due to the flaw. A brief description of the problem formulation is presented below summarizing a more detailed account given elsewhere [4].

As illustrated in Fig. 1, the coordinate system is chosen such that the surface of the conductor lies in the plane $y = 0$ and the crack lies in the plane $z = 0$. The electric field in the conductor is decomposed into transverse electric (TE) and transverse magnetic (TM) modes defined with respect to the normal to the crack. Assuming that the electromagnetic field varies as the real part of $\exp(-i\omega t)$, this decomposition is written [5]

$$\boldsymbol{E}(\boldsymbol{r}) = i\omega\mu_0\mu_r\left[\nabla \times \hat{z}\psi'(\boldsymbol{r}) - \nabla \times \nabla \times \hat{z}\psi''(\boldsymbol{r})\right] \quad (1)$$

where

$\hat{z}$ z-directed unit vector;
ψ' TE Hertz potential;
ψ'' corresponding TM potential.

It is more usual in a scalar reduction of a half-space electromagnetic field to choose the preferred direction as the direction normal to the interface. The normal to the crack is selected here because this means that only the TM mode interacts directly with an ideal crack of negligible opening.

If the crack has a finite opening, there is direct TE interaction even though the current is incident edge-on. The approach taken here is to determine the field for the case of a crack of negligible opening and neglect direct perturbation of the TE field. Indirect perturbation of the TE field occurs through the cross-coupling between TE and TM modes at the air-conductor interface, and this is taken into account implicitly through the integral kernels that are used.

Assuming that a crack at open surface S_0 is a perfect barrier to electric current, the normal component of the electric field at the crack face is zero. Putting

$$\boldsymbol{E}(\boldsymbol{r}) \cdot \hat{z} = 0, \qquad \boldsymbol{r} \in S_0 \quad (2)$$

in (1) shows that

$$\nabla_z^2 \psi''(\boldsymbol{r}) = 0, \qquad \boldsymbol{r} \in S_0 \quad (3)$$

where $\nabla_z^2 = (\partial^2/\partial x^2) + (\partial^2/\partial y^2)$ is the Laplacian operator defined for a surface transverse to the z direction. Thus the TM potential $\psi''(\boldsymbol{r})$ satisfies a two-dimensional (2-D) Laplace equation on the crack face regardless of the frequency of excitation or the skin depth.

B. Boundary Conditions

In order to find a solution of (3), boundary conditions at the perimeter of the crack face are needed. Although the general case of arbitrary frequency is tractable [6], the problem can be simplified by considering the field at high frequencies where the skin depth is small compared with the dimensions of the crack face. Two boundary conditions have been derived for the thin-skin regime; one which applies at the buried edge of the crack and the other at the crack mouth.

1) Edge Boundary Condition: Following other authors who have considered the thin-skin regime [2], [7]–[10], the magnetic field in the plane of the crack normal to the edge is taken to be zero. Applying this condition to the TM field gives

$$\boldsymbol{H}_{\mathrm{TM}}(x_e, y_e) \cdot \hat{n} = 0 \quad (4)$$

where the subscript e refers to points at the crack edge and $\hat{n}$ is a unit vector in the plane of the crack, normal to the edge. Because it is only necessary to consider the field in the plane $z = 0$, reference to the zero z coordinate is suppressed. The TM magnetic field in the plane of the crack is given by

$$\boldsymbol{H}_{\mathrm{TM}}(x, y) = \nabla \times [\hat{z}\psi(x, y)] \quad (5)$$

where $\psi(x, y) = -k^2\psi''(x, y)$ with $k^2 = i\omega\mu_0\mu_r\sigma$. Hence the edge condition, (4), implies that the derivative of ψ with respect to a coordinate tangential to the edge is zero. Integrating with respect to this edge coordinate and setting the arbitrary integration constant to zero gives

$$\psi(x_e, y_e) = 0 \quad (6)$$

at the crack edge.

2) Mouth Boundary Condition: The mouth boundary condition is more problematic. In general, the x component of the magnetic field can be expressed as the sum of an incident and a scattered field

$$H_x(x, y) = H_x^{(i)}(x, y) + H_x^{(s)}(x, y) \quad (7)$$

where the superscript (i) denotes the known incident field and (s) refers to the scattered field. Similarly, the corresponding relationship for the TM potential is written as

$$\frac{\partial\psi}{\partial y} = \frac{\partial\psi^{(i)}}{\partial y} + \frac{\partial\psi^{(s)}}{\partial y}. \quad (8)$$

According to Auld's approximation, the scattered field at the mouth of the crack is neglected, but for more accurate predictions [3] its effect must be retained. By writing the scattered field in integral form and considering points at the crack mouth it is found that [3]

$$\left.\frac{\partial\psi(x, y)}{\partial y}\right|_{y=0} = \left.\frac{\partial\psi^{(i)}(x, y)}{\partial y}\right|_{y=0} + \frac{2}{ik}\int_{-a}^{a} \frac{\partial^2}{\partial x^2} U(x - x')\psi(x', 0)\, dx' \quad (9)$$

where $2a$ is the surface length of the crack $-a \le x \le a$, and

$$U(x) = \frac{\mu_r k^4}{(2\pi)^2} \int_{-\infty}^{\infty}\int_{-\infty}^{\infty} \frac{1}{w^2 - k^2}\left(\frac{1}{\kappa} - \frac{\mu_r}{\gamma}\right) \times \frac{1}{[(\mu_r^2 - 1)\kappa^2 + k^2]}\, e^{iux}\, du\, dw \tag{10}$$

with $\kappa^2 = u^2 + w^2$, $\gamma = \sqrt{u^2 + w^2 - k^2}$, and the root with a positive real part is taken.

Note that the boundary condition (9) is derived from an integral equation that represents the jump in the electric field at the crack in terms of a surface dipole density [4]. A thin-skin relationship, equivalent to the impedance boundary condition, is used to eliminate the dipole density inside the integral in favor of the TM potential, see [4, eq. (23)]. Although the derivation of (9) involves a thin-skin assumption, the half-space kernel $U(x-x')$ given in (10), has not been simplified using the same assumption. This is because there is no significant advantage gained when solving (9).

III. Probe Impedance

The change in the impedance of an eddy-current probe ΔZ due to a crack is commonly defined in terms of the perturbed field at the excitation coil. This relationship is transformed using reciprocity principles and the impedance boundary condition to give a more convenient form for computation from a knowledge of the TM potential [4]. Although the TM potential is determined for a crack of zero opening, the derivation of the impedance allows for the effects of a small crack gape c, and the possibility that the crack is filled with a nonconducting material of relative permeability μ_c, which may differ from the permeability of the host material μ_r. The impedance is written as

$$\Delta Z = Z_F + Z_S + Z_K \tag{11}$$

where, for unit coil current

$$Z_F = -\frac{1}{\sigma}\left(k^2 c\,\frac{\mu_c}{\mu_r} + 2ik\right)\int_{-a}^{a} H_x^{(i)}(x, 0)\psi(x, 0)\, dx \tag{12}$$

$$Z_S = \frac{ikc}{\sigma}\int_{-a}^{a} H_x^{(i)}(x, 0)[H_x(x, 0) - H_{t\mathrm{TM}}(x, y_e)]\, dx \tag{13}$$

and

$$\begin{aligned} Z_K = &-\frac{4}{\pi\sigma}\int_{-a}^{a} H_x^{(i)}(x, 0)H_x(x, 0)\, dx \\ &-\frac{4}{\pi\sigma}\int_{-a}^{a} H_x^{(i)}(x, 0)H_{x\mathrm{TM}}(x, 0)\, dx \\ &+\frac{1}{\sigma}\int_{-a}^{a} H_x^{(i)}(x, 0)H_{t\mathrm{TM}}(x, y_e)\,\mathrm{cosec}\,\theta\, dx. \end{aligned} \tag{14}$$

The expression for Z_F, (12), can be interpreted as the sum of a volume term of order $(ik)^2$ and a surface term of order ik. The loss of surface at the crack mouth and the additional surface at the crack base give rise to the contribution Z_S, where $H_{t\mathrm{TM}}$ is the TM magnetic field tangential to the crack edge in the $z = 0$ plane. As with the surface term in Z_F, the factor ik in Z_S indicates that it can be derived with reference to the impedance boundary condition [2] or an equivalent approach [4]. Finally, corrections of order $(ik)^0$ due to Kahn effects at the crack mouth and the edge are contained in Z_K [4], [11]. In the expression for the edge effect, represented by the third integral in (14), the angle θ is as shown in Fig. 2(a).

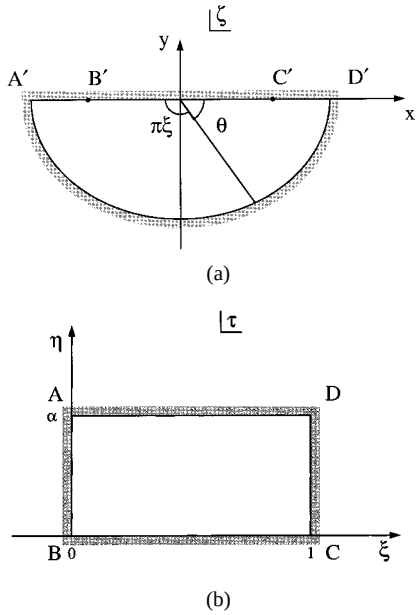

Fig. 2. (a) Semielliptical crack domain and (b) rectangular domain defined by mapping the semiellipse.

In order to compute the impedance from (11)–(14), it is necessary to calculate the potential ψ and the magnetic field. These calculations have been performed for long cracks of uniform depth [4] and for rectangular cracks [12]. Below, the formalism is adapted to deal with curved crack profiles.

IV. Semielliptical Crack

A. Mapping to a Rectangle

Consider a semielliptical crack with a semimajor axis of length a and a semiminor axis of length b whose surface normal is in the z direction [Fig. 2(a)]. By mapping the semiellipse to a rectangle, a simple series expansion can be used to represent the solution. The mapping is introduced by first noting that the ellipse can be represented in parametric form as

$$x = a\cos\theta \tag{15}$$

$$y = -b\sin\theta \tag{16}$$

where θ is the angle between the x axis and a line drawn from the center of the ellipse. Rather than using the variable θ, it will be advantageous to put

$$\theta = \pi(1 - \xi) \tag{17}$$

and express the relationships in (15) and (16) in terms of the complex variable $\zeta = x + iy$. Define parameters K and α such that

$$a = K\cosh(\pi\alpha) \tag{18}$$

and

$$b = K \sinh(\pi\alpha) \tag{19}$$

where $x = \pm K$ locates the focal points. Put

$$\zeta = x + iy = K \cos[\pi(1-\tau)] \tag{20}$$

where $\tau = \xi + i\eta$. Equations (15) and (16) are recovered by putting $\eta = \alpha$, and equating real and imaginary parts. Equation (20) maps a semiellipse in the half-plane $y < 0$ to a rectangular region, Fig. 2, in the complex plane of the variable τ. Consideration of how the boundary of the semiellipse maps to the τ-domain gives rise to a number of useful relationships. These will be derived while noting the correspondence between parts of the boundary of the semiellipse and each side of the rectangle AB, BC, CD, and DA in turn [Fig. 2(b)].

The inverse of the mapping defined by (20) is given by

$$\tau = 1 - \frac{1}{\pi} \arccos(\zeta/K) \tag{21}$$

and is made single-valued by selecting the principal value of the inverse cosine function. Thus in (21) the function $\arccos(\zeta/K)$ is defined with its real part in the range 0 to π.

B. Mapping Points on the Crack Perimeter

In transforming points on the line of the crack mouth, A′D′ in Fig. 2, it is helpful to write (21) for $y = 0$ in the form [13, eqs. (4.4.11) and (4.4.38)]

$$\tau = 1 + \frac{i}{\pi} \ln\left[x/K + \sqrt{(x/K)^2 - 1}\right]. \tag{22}$$

The mouth line, divided into three parts by the foci, transforms piecewise as follows.

For $-a/K \le x/K \le -1$ with $y = 0$, corresponding to the line A′B′ in Fig. 2(a), then the argument of the natural logarithm in (22) is a negative real number which means that the real part of the RHS of (22) vanishes. Consequently $\xi = 0$ and

$$\begin{aligned}\eta &= \frac{1}{\pi} \ln\left[-x/K - \sqrt{(x/K)^2 - 1}\right] \\ &= \frac{1}{\pi} \operatorname{arccosh}(x/K).\end{aligned} \tag{23}$$

For $-1 \le x/K \le 1$ with $y = 0$, corresponding to B′C′ in Fig. 2(a), it can be seen from (21) that τ is real. This means that $\eta = 0$ and

$$\xi = 1 - \frac{1}{\pi} \arccos(x/K). \tag{24}$$

For $1 \le x/K \le a/K$ and $y = 0$, corresponding to C′D′ in Fig. 2(a), equating the real and imaginary parts of (22) gives $\xi = 1$ and

$$\eta = \frac{1}{\pi} \operatorname{arccosh}(x/K). \tag{25}$$

Expressions (23)–(25) are derived from (22) using the identities [13, eqs. (4.4.27) and (4.6.21)]

$$\arccos x = -i \ln\left(x^2 + \sqrt{x^2 - 1}\right), \qquad x^2 \le 1 \tag{26}$$

$$\operatorname{arccosh} x = \ln\left(x + \sqrt{x^2 - 1}\right), \qquad x \ge 1. \tag{27}$$

Finally, on the elliptical boundary $\eta = \alpha$ and, from (15) and (17)

$$\xi = 1 - \frac{1}{\pi} \arccos(x/a) \tag{28}$$

where $-1 \le x/a \le 1$.

C. Formal Solution

It is easy to construct a series solution of the Laplace equation in a rectangular domain if the potential, or its normal gradient, vanishes on three sides of the rectangle. To take advantage of this facility, the solution for a semielliptical crack is written as

$$\psi = \psi_1 + \psi_2 \tag{29}$$

where both ψ_1 and ψ_2 satisfy the Laplace equation. The first function ψ_1 is the solution for a rectangular crack whose length and depth equal those of the semiellipse. The second function ψ_2 corrects for the fact that the actual crack domain is not rectangular.

With the TM potential expressed as in (29), the edge boundary condition, (6), is easily satisfied by demanding that

$$\psi_1(x_e, y_e) + \psi_2(x_e, y_e) = 0 \tag{30}$$

but once again the mouth boundary condition presents a difficulty. Substituting (29) into (9) gives an equation coupling ψ_1 and ψ_2 at the boundary. However, it is desirable to satisfy the edge boundary condition in such a way that one of the two solutions can be found independently of the other. This is difficult to accomplish if exact compliance with (9) is demanded, and for this reason an approximation is used.

As matter of choice, let

$$\frac{\partial \psi_2}{\partial y} = 0, \qquad -a \le x \le a,\ y = 0 \tag{31}$$

apply at the crack mouth. As a consequence, the normal gradient of ψ_2 vanishes on three sides of the rectangle in the transformed domain. By solving first for ψ_1, as described below, (30) gives a Dirichlet condition for ψ_2 on the fourth side of the rectangle.

An approximate mouth boundary condition for ψ_1 is obtained by substituting (29) and (31) into (9), using (31) and neglecting ψ_2 in the integral term. This gives

$$\left.\frac{\partial \psi_1}{\partial y}\right|_{y=0} = \left.\frac{\partial \psi^{(i)}}{\partial y}\right|_{y=0} + \frac{2}{ik} \int_{-a}^{a} \frac{\partial^2}{\partial x^2} U(x - x') \psi_1(x', 0)\, dx'. \tag{32}$$

It is reasonable to neglect ψ_2 in the integral first because ψ_2 is much smaller than ψ_1 at the mouth of the crack and second because the integral operator makes a contribution to the right-hand side of (32) that is much smaller than the incident field term.

The potential ψ_1 is set to zero at three sides of a rectangle in ordinary configuration space. Thus

$$\psi_1 = 0, \qquad \begin{cases} x = \pm a, & 0 \le y \le b \\ -a < x < a, & y = b. \end{cases} \tag{33}$$

This means that ψ_1 has the same boundary conditions as the solution for a rectangular crack and can therefore be calculated in

the same way [12]. Once ψ_1 is known, (30) is used to determine the edge condition on ψ_2. Writing $\psi_1 = -F(x_e, y_e)$ for points on the elliptical boundary, (30) is satisfied by putting

$$\psi_2(x_e, y_e) = F(x_e, y_e). \tag{34}$$

The 2-D Laplace equation for ψ_2 on the semielliptical domain can now be solved according to boundary conditions (31) and (34). The solution proceeds by mapping ψ_2 to a rectangle in the τ-domain using (21). The edge maps to the line $\eta = \alpha$ in the τ-domain with $0 \le \xi \le 1$. Let $F(x_e, y_e)$ map to a function $f(\xi)$ on this line. Then, in mapping ψ_2 to the τ-domain such that

$$\psi_2(x, y) = \phi[\xi(x, y), \eta(x, y)] \tag{35}$$

it is required that

$$\phi(\xi, \alpha) = f(\xi) \quad \text{with} \quad 0 \le \xi \le 1 \tag{36}$$

while at the other three sides of the rectangle, the normal gradient is zero

$$\frac{\partial \phi}{\partial \xi} = 0, \qquad \xi = 0 \text{ or } 1,\ 0 \le \eta \le \alpha \tag{37}$$

$$\frac{\partial \phi}{\partial \eta} = 0, \qquad 0 \le \xi \le 1,\ \eta = \alpha. \tag{38}$$

This completes the definition of the boundary conditions needed to find ψ_1 and ψ_2.

D. Series Solutions

The solution of the Laplace equation for ψ_1 in the rectangular domain is written

$$\psi_1(x, y) = -\sum_n D_n \times \frac{2a \sin[(n\pi/2)(x/a+1)] \sinh[(n\pi/2)(b-y)/a]}{n\pi \cosh(n\pi b/2a)}. \tag{39}$$

Note that this vanishes for $x = \pm a$ and for $y = b$ as required by (33). The normal derivative at the crack mouth, given by

$$\left.\frac{\partial \psi_1(x, y)}{\partial y}\right|_{y=0} = \sum_n D_n \sin[(n\pi/2)(x/a+1)] \tag{40}$$

is substituted into (32) and the expansion coefficients D_n are calculated by solving a matrix equation. To obtain the matrix equation, (32) is multiplied by $\sin[(m\pi/2)(x/a+1)]$, the resultant relationship integrated from $-a$ to a and the orthogonality properties of the sine function used to define a system of linear equations as described in [12]. A solution of the linear system is found by LU decomposition [14].

In the τ-domain, the required solution is

$$\phi(\xi, \eta) = \sum_n C_n \frac{\cos(n\pi\xi) \cosh(n\pi\eta)}{\cosh(n\pi\alpha)}. \tag{41}$$

TABLE I
EPI-CYCLE COORDINATES

Point	τ	x
A	$i\alpha$	$\sum_\nu (-1)^\nu K_\nu \cosh(\nu\pi\alpha)$
B	0	$\sum_\nu (-1)^\nu K_\nu$
C	1	$\sum_\nu K_\nu$
D	$1 + i\alpha$	$\sum_\nu K_\nu \cosh(\nu\pi\alpha)$

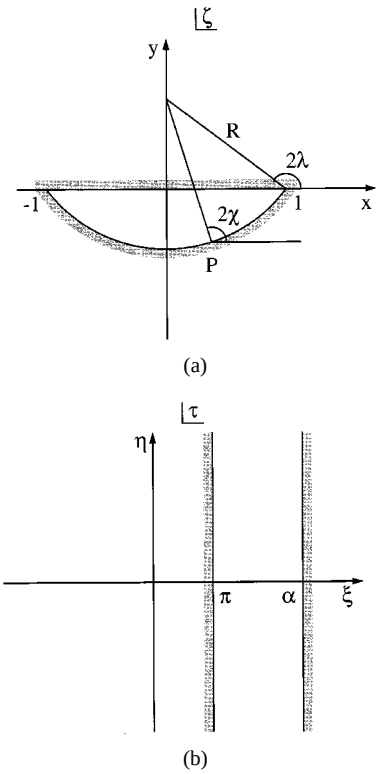

Fig. 3. (a) Circular arc crack and (b) solution domain defined by mapping the region of the arc crack to an infinite strip such that $\pi \le \xi \le \alpha$.

Note that the normal derivative of the potential on three sides of the rectangle vanishes in accordance with (37) and (38). For $\eta = \alpha$

$$\phi(\xi, \alpha) = \sum_n C_n \cos(n\pi\xi) \tag{42}$$

and the derivative with respect to η at $\eta = \alpha$ is given by

$$\left.\frac{\partial \phi(\xi, \eta)}{\partial \eta}\right|_{\eta=\alpha} = \sum_n C_n n\pi \cos(n\pi\xi) \tanh(n\pi\alpha). \tag{43}$$

This derivative is needed to calculate $H_{t\mathrm{TM}}$ at the crack edge as required for the evaluation of (14). From (36) and (42)

$$C_m = 2\int_0^1 f(\xi) \cos(m\pi\xi)\, d\xi. \tag{44}$$

The procedure outlined in this section gives the TM potential for a semielliptical crack. A variation of this analysis has been used for elliptical epicyclic cracks as follows.

V. SEMIELLIPTICAL EPICYCLIC CRACK PROFILE

Consider a crack that has a smooth profile intersecting the surface of the conductor at right angles (Fig. 1). This type of crack

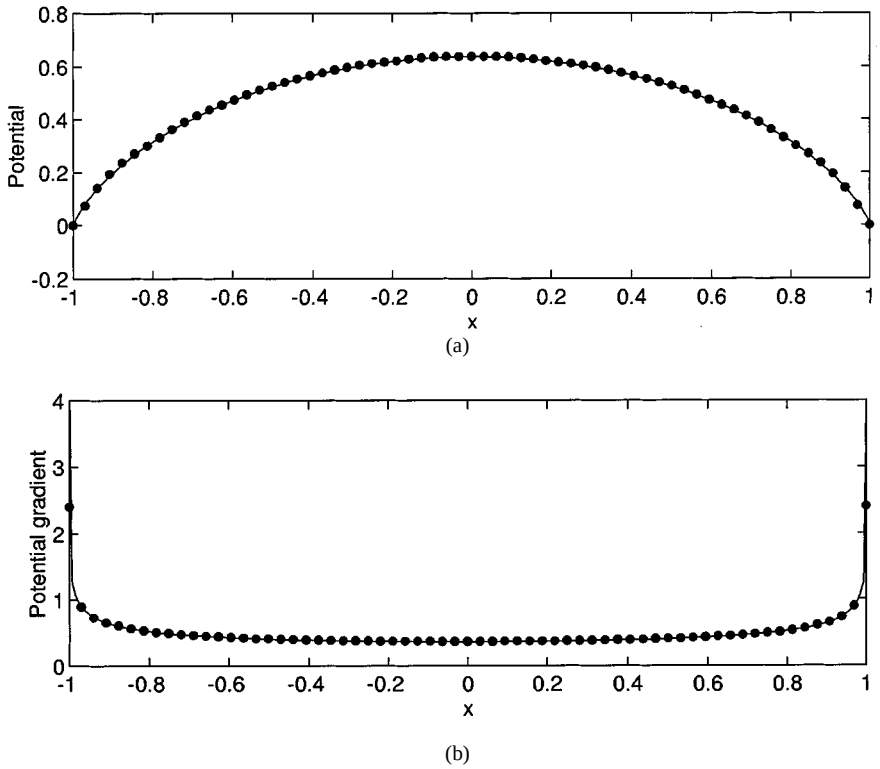

Fig. 4. Potential and potential gradient at the mouth of a semicircular crack in a uniform field: comparison of an analytical solution (continuous line) with results computed by Fourier expansion (circles).

can occur in practice when two semielliptical cracks merge. Crack shapes of this type, which include the semiellipse as a special case, can be approximated by a series of nested elliptical epicycles. Generalizing (15) and (16) and using (17), the crack profile is represented in parametric form as

$$x = \sum_{\nu} a_\nu \cos[\nu\pi(1-\xi)] \tag{45}$$

$$y = \sum_{\nu} b_\nu \sin[\nu\pi(1-\xi)] \tag{46}$$

with $\nu = 1, 2, \ldots, N$. In order to define a suitable transformation from the ζ to the τ-domain, Fig. 2, write

$$a_\nu = K_\nu \cosh(\nu\pi\alpha) \tag{47}$$

and

$$b_\nu = K_\nu \sinh(\nu\pi\alpha). \tag{48}$$

Then with $\zeta = x + iy$ define

$$\zeta = \sum_{\nu} K_\nu \cos[\nu\pi(1-\tau)]. \tag{49}$$

The four corners of the rectangular region in the τ-domain correspond to the ends of the crack and the focal points. The x coordinates of these points are related to expansion parameters as given in Table I. Define two new parameters λ_+ and λ_- such that their reciprocals are the x coordinates of the foci. Then

$$1/\lambda_\pm = \pm \sum_{\nu} (\pm 1)^\nu K_\nu. \tag{50}$$

TABLE II
COIL PARAMETERS

Outer radius	7.50 ± 0.05 mm
Inner radius	2.51 ± 0.01 mm
Axial length	4.99 ± 0.01 mm
Nominal lift-off	0.10 ± 0.01 mm
Number of turns	4000 ± 1 mm

Note that the length of the crack is given by

$$a = 2 \sum_{n} K_{2n-1} \cosh[(2n-1)\pi\alpha]$$
$$= 2 \sum_{n} a_{2n-1}, \qquad 2n-1 \le N \tag{51}$$

and the center of the crack mouth is located at $x = x_0$ where

$$x_0 = \sum_{n} a_{2n}, \qquad 2n \le N. \tag{52}$$

Clearly, if $N = 1$, then these expressions reduce to those for the semiellipse.

VI. CALCULATIONS AND VALIDATION

In order to validate the predictions, comparisons have been made with analytical results for a semicircular crack in a uniform field and with experimental measurements of coil impedance for a number of slots in aluminum plates. The solution for a semicircular crack is derived as a special case of the circular-arc crack solution described in the Appendix. Using Auld's approximate boundary condition, three analytical

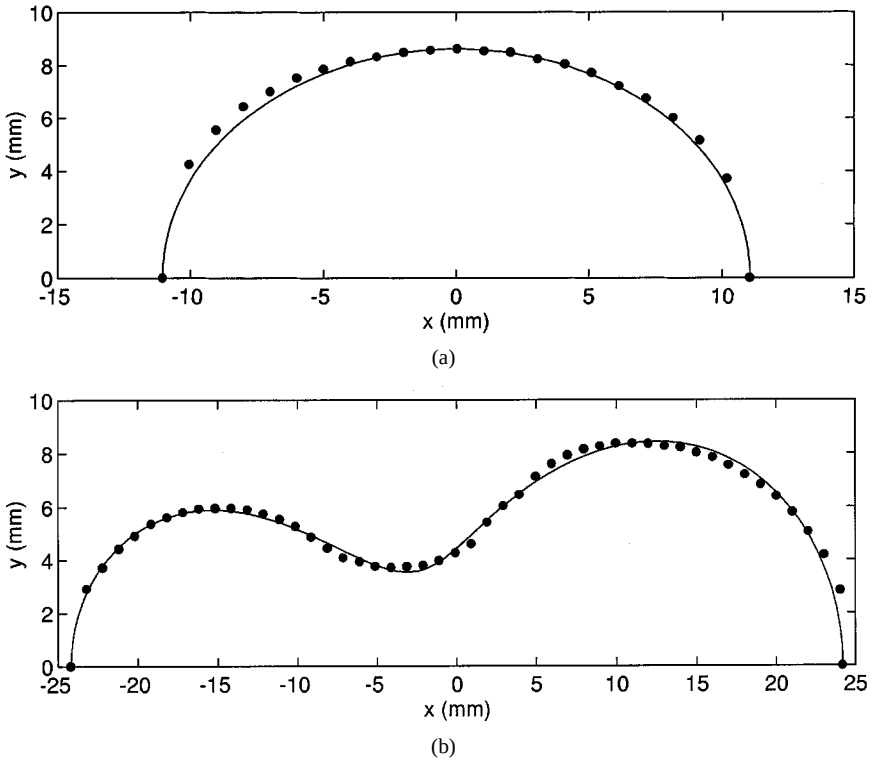

Fig. 5. Comparison of crack edge coordinates with the profile representation used for mapping. (a) Slot D1 is approximated in the calculation as a semiellipse. (b) Slot D2 is approximated as a fifth-order elliptical epi-cycle.

results have been derived allowing comparisons with the computed results of the expansion method, Section IV-D.

The circular arc crack problem is solved by conformal mapping of a region bounded by the arc and its chord to an infinite strip parallel to the imaginary axis in the transformed domain, Fig. 3. The solution is written

$$\psi(x, y) = \phi[\xi(x, y), \eta(x, y)] \tag{53}$$

where ϕ is the potential in the domain of the strip. The chord maps to a line $\xi = \pi$ and the arc to a line $\xi = 3\pi/2$. For the first comparison, the potential at the chord is used, given by

$$\psi(\pi, \eta) = \frac{2\eta}{\pi \sinh \eta} \tag{54}$$

with $e^{\eta} = (1+x)/(1-x)$. This is compared with the results of the expansion method with the Auld approximation, Fig. 4(a). Second, the magnetic field at the edge of the circular arc crack, which can be deduced from

$$\left.\frac{\partial \psi}{\partial \xi}\right|_{\xi=3\pi/2} = \frac{2}{\pi}(1 - \eta \tanh \eta)\operatorname{sech}\eta - \operatorname{sech}^2 \eta \tag{55}$$

with $e^{\eta} = \tan(\chi)$, is compared with the results of the expansion method in Fig. 4(b). Note that the angle λ is shown in Fig. 3.

From (12), the dominant impedance term for a semicircular crack of radius a and zero opening in a uniform incident magnetic field H_0, can be written as

$$Z_F = -\frac{2ik}{\sigma} a^2 H_0^2 Z_0 \tag{56}$$

for unit coil current, where Z_0 is a dimensionless normalized impedance. Note that the impedance depends on the square of the crack radius and therefore depends on its area. In the Appendix it is shown that

$$Z_0 = \left(\frac{\pi}{2} - \frac{2}{\pi}\right). \tag{57}$$

Hence $Z_0 = 0.9342$ to four significant figures. This is in close agreement with the result from the expansion method 0.9350 with 20 terms in the summations.

Impedance predictions have been compared with experimental measurements made by Harrison *et al.* [15] on electro-discharge machined slots in aluminum plates. The coil parameters for these experiments are listed in Table II. Calculation of the incident coil field is performed using a well-known integral expression [16]. Parametric representations of two of the slots used in the experiments of Harrison *et al.*are compared with slot profile measurements in Fig. 5. Two further slots are shown in Fig. 6. The undulating shapes shown in Figs. 5(b) and 6(b) were approximated using fifth-order epicycles to facilitate mapping to a rectangular domain. Parameters of the epicycles were found by a least-squares fit to the measured slot profiles and are given in Table III. Other slot parameters are given in Table IV together with probe lift-off values.

A comparison between theory and experiment at the highest excitation frequency, 50 kHz, for a near semielliptical simulated crack [Fig. 5(a)] is shown in Fig. 7. The calculated resistance variation shows good agreement with experimental data, while

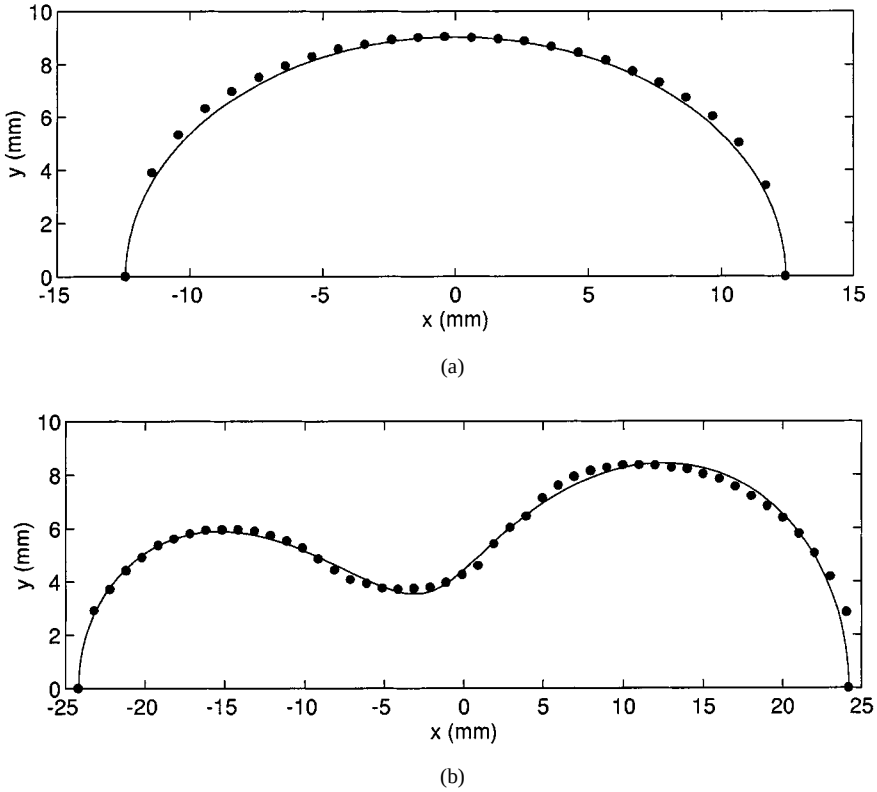

Fig. 6. Comparison of crack edge coordinates with the profile representation used for mapping. (a) Slot D3 is approximated as a semiellipse. (b) Slot D4 is approximated as a fifth-order elliptical epi-cycle.

TABLE III
EPI-CYCLE PARAMETERS

Parameter	Slot D2	Slot D4
a(1) (mm)	22.093	19.252
a(2) (mm)	−2.526	1.622
a(3) (mm)	3.354	4.422
a(4) (mm)	−0.083	0.624
a(5) (mm)	−0.570	0.529
b(1) (mm)	7.400	6.528
b(2) (mm)	−1.522	0.986
b(3) (mm)	2.616	3.473
b(4) (mm)	−0.074	0.554
b(5) (mm)	−0.536	0.499

TABLE IV
SLOT PARAMETERS

Parameter	Slot D1	Slot D2	Slot D3	Slot D4
Length (mm)	22.10 ± 0.05	49.78 ± 0.05	24.84 ± 0.05	48.41 ± 0.05
Max depth (mm)	8.61 ± 0.05	8.94 ± 0.05	9.04 ± 0.05	8.36 ± 0.05
Max opening (mm)	0.33 ± 0.01	0.37 ± 0.01	0.32 ± 0.01	0.30 ± 0.01
Conductivity (MS/m)	22.50 ± 0.05	22.40 ± 0.05	23.15 ± 0.05	23.20 ± 0.05
Coil lift-off (mm)	0.491 ± 0.01	0.318 ± 0.01	0.368 ± 0.01	0.498 ± 0.01

the agreement between the predicted and measured self-inductance is excellent. Calculations have also been performed to determine the impedance due to the simulated crack with an undulating profile shown in Fig. 5(b). The comparison between calculated and measured probe response for this flaw (Fig. 8) again shows good agreement between predictions and experiment. Comparisons between predictions and experiment for the two further slots (Fig. 6) are shown in Figs. 9 and 10.

VII. CONCLUSION

A central aim of the present theory is to predict high-frequency probe impedance variations due to eddy-current interactions with cracks in materials of arbitrary permeability taking into account the perturbation of the field at the crack mouth. The starting point of this thin-skin theory is a vector potential formulation of the crack problem which yields an integral equation valid at arbitrary frequency [6]. In solving the general equation, a solution of the surface Laplace equation must be found and, simultaneously, the discontinuity in the electromagnetic field at the crack must be found. The discontinuity in the tangential electric field was represented in terms of a surface dipole layer [6] which could be computed by calculating the numerical solution of an integral equation. Subsequently, the vector potential formulation was recast using Hertz potentials and specialized for the high-frequency regime [4]. In this regime, the dipole density drops out of the problem because it is simply proportional to the Laplacian potential. This means that only one unknown surface function is required; the TM potential at the crack face.

The TM potential has been evaluated using a boundary condition valid for arbitrary permeability which takes into account

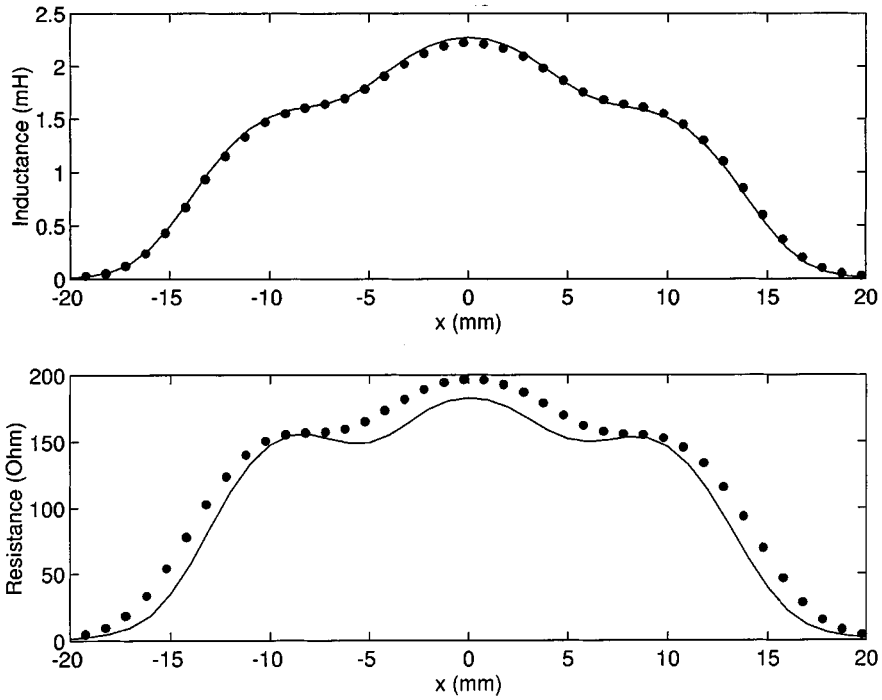

Fig. 7. Comparison of probe impedance predictions with experimental measurements for slot D1, approximated as a semiellipse.

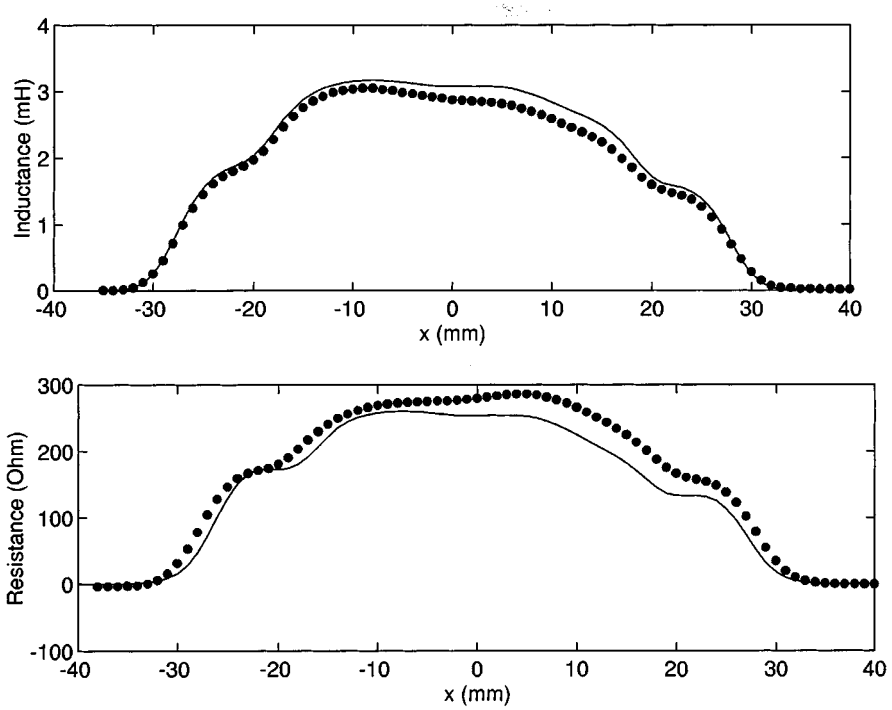

Fig. 8. Comparison of probe impedance predictions with experimental measurements for slot D2.

the perturbation of the magnetic field at the crack mouth. Included in the impedance calculation are terms that represent the effects of crack opening. In addition, Kahn-level terms are used which have the correct reciprocal form [4]; they involve integrals of products of an unperturbed field and the total field. This contrasts with earlier attempts to account for Kahn effects [2], [8]. Calculations have been performed to test the accuracy of the predictions by comparing the results with an analytical solution and with experimental measurements. These have demonstrated that the numerical calculations are both rapid and accurate.

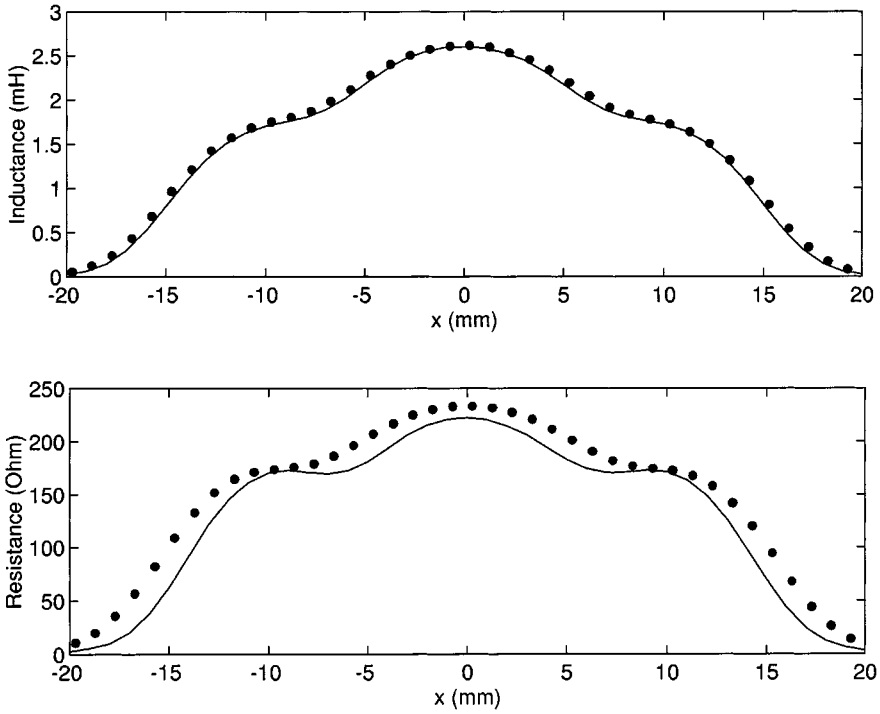

Fig. 9. Comparison of probe impedance predictions with experimental measurements for slot D3, approximated as a semiellipse.

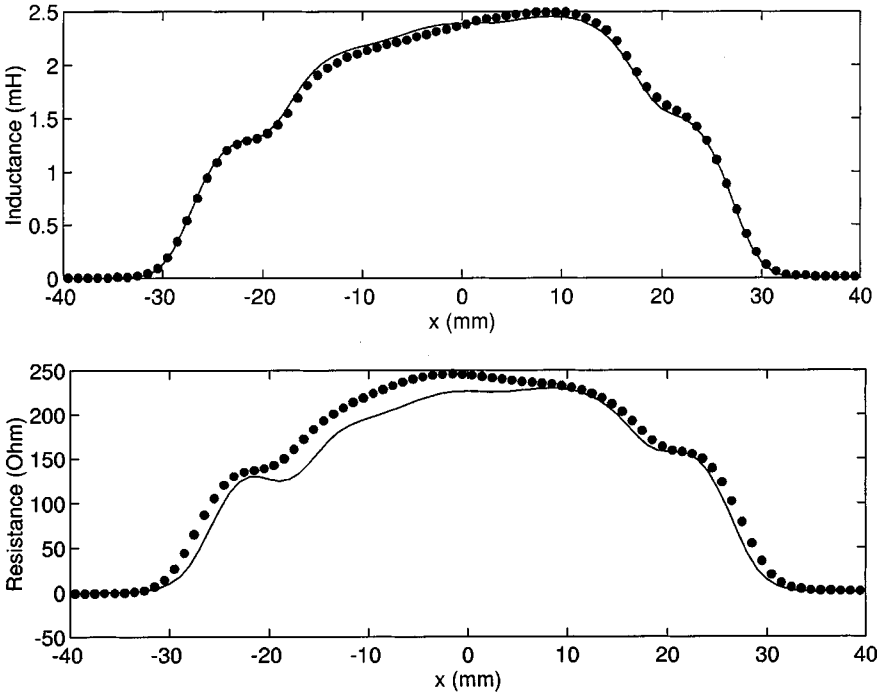

Fig. 10. Comparison of probe impedance predictions with experimental measurements for slot D4.

APPENDIX
THE CIRCULAR ARC CRACK

A mapping applicable to cracks bounded by a circular arc and a chord (Fig. 3) has been considered by McIver [17] in a study of an inverse problem. For a semicircular crack in a uniform unperturbed field, an analytical solution can be derived by applying Auld's approximate boundary condition. By scaling the field, the boundary condition at the chord is written

$$\frac{\partial \psi}{\partial y} = 1 \tag{A1}$$

and on the circular arc

$$\psi = 0 \tag{A2}$$

as before.

The required mapping is given by

$$\zeta = i\,\cot(\tau/2) \tag{A3}$$

for a chord whose half-length is unity. The inverse mapping can be expressed as

$$\tau = -i\,\ln\left(\frac{\zeta-1}{\zeta+1}\right). \tag{A4}$$

For points on the chord, $\zeta = x$ with $|x| \le 1$. Putting $\tau = \xi + i\eta$ and equating the real and imaginary parts of (A4) for such points gives $\xi = \pi$ and $\eta = \ln(1+x)/(1-x)$. Hence, that part of the real axis in the ζ-plane from $x = -1$ to $x = 1$, corresponding to the crack mouth, maps to a line in the τ plane parallel to the η axis passing through the ξ axis at $\xi = \pi$.

In order to elucidate the mapping of the circular arc, note that by using the notation of Fig. 3

$$\zeta - 1 = R\left[e^{i2\lambda} - e^{i2\chi}\right]$$

and

$$\zeta + 1 = R\left[e^{i(\pi-2\lambda)} - e^{i2\chi}\right] \tag{A5}$$

for an arbitrary point on an arc of radius R. Hence from (A4)

$$\tau = i\,\ln\left[-\frac{\cos(\lambda+\chi)}{\sin(\lambda-\chi)}\right] + 2\lambda + \frac{\pi}{2}. \tag{A6}$$

The argument of the natural logarithm lies in the range zero (for $x = -1$, $\lambda+\chi = \pi/2$) to infinity (for $x = 1$, $\lambda-\chi = 0$) hence the arc maps to a line in the τ plane parallel to the η axis and passing through the point $\xi = 2\lambda+(\pi/2) = \alpha$. For a semicircle, $\lambda = \pi/2$ and the argument of the natural logarithm reduces to $\tan\,\chi$. Hence, from the imaginary part of (A6), $\eta = \ln(\tan\,\chi)$ and the arc maps to a line parallel to the η axis crossing the real axis at $\xi = 3\pi/2$.

The required solution is written as

$$\psi(x, y) = \phi[\xi(x, y), \eta(x, y)] \tag{A7}$$

where [17]

$$\phi(\xi, \eta) = \int_{-\infty}^{\infty} \frac{\sinh[k(\alpha-\xi)]}{\sinh(k\pi)\,\cosh[k(\alpha-\pi)]}\,e^{-ik\eta}\,dk. \tag{A8}$$

For a semicircular arc, $\alpha = 3\pi/2$ and the potential on the line $\xi = \pi$ may be evaluated to give [18]

$$\phi(\pi, \eta) = \frac{2\eta}{\pi\,\sinh\,\eta}. \tag{A9}$$

It is also of interest to evaluate the gradient of the potential at the line of the arc since this is of relevance to the calculation of the edge field. For a semicircular crack, it is found that

$$\left.\frac{\partial\phi}{\partial\xi}\right|_{\xi=3\pi/2} = \frac{2}{\pi}\,(1-\eta\,\tanh\,\eta)\,\mathrm{sech}\,\eta - \mathrm{sech}^2\,\eta. \tag{A10}$$

The normalized probe impedance is defined by

$$Z_0 = \int_{-1}^{1} \psi f\,dx \tag{A11}$$

where f is the prescribed unperturbed field. This definition may be compared with (12) of the main text with a multiplying factor removed in the process of normalizing. For a uniform incident field $f = 1$ and with ψ given by (A7) and (A9)

$$\begin{aligned} Z_0 &= \int_{-\infty}^{\infty} \phi\,\frac{\partial x}{\partial\eta}\,d\eta \\ &= \frac{2}{\pi}\int_{-\infty}^{\infty} \frac{\eta}{(1+\cosh\,\eta)\,\sinh\,\eta}\,d\eta \end{aligned} \tag{A12}$$

which may be evaluated to give

$$Z_0 = \left(\frac{\pi}{2} - \frac{2}{\pi}\right). \tag{A13}$$

In the main text this result is compared with calculations carried out using the Fourier expansion method for a semielliptical crack that approximates a semicircle.

REFERENCES

[1] B. A. Auld, F. G. Muennemann, and M. Riaziat, *Research Techniques in Nondestructive Testing*, R. S. Sharpe, Ed. London, U.K.: Academic, 1984, vol. 7, ch. 2.

[2] B. A. Auld, S. R. Jefferies, and J. C. Moulder, "Eddy-current signal analysis and inversion for semielliptical surface cracks," *J. Nondestr. Eval.*, vol. 7, pp. 79–94, 1988.

[3] N. Harfield and J. R. Bowler, *Electromagnetic Nondestructive Evaluation*, T. Takagi, J. R. Bowler, and Y. Yoshida, Eds. Amsterdam, The Netherlands: IOS, 1997, pp. 59–66.

[4] ——, "Theory of thin-skin eddy-current interaction with surface cracks," *J. Appl. Phys.*, vol. 82, no. 9, pp. 4590–4603, 1997.

[5] L. B. Felsen and N. Marcuvitz, *Radiation and Scattering of Waves*. Englewood Cliffs, NJ: Prentice-Hall, 1973.

[6] J. R. Bowler, Y. Yoshida, and N. Harfield, "Vector potential boundary integral evaluation of eddy-current interaction with a crack," *IEEE Trans. Magn.*, vol. 33, pp. 4287–4294, Sept. 1997.

[7] A. M. Lewis, "A theoretical model of the response of an eddy-current probe to a surface-breaking metal fatigue crack in a flat test piece," *J. Phys. D: Appl. Phys.*, vol. 25, pp. 319–326, 1992.

[8] S. K. Burke, "Eddy-current inversion in the thin-skin limit: Determination of depth and opening for a long crack," *J. Appl. Phys.*, vol. 76, pp. 3072–3080, 1994.

[9] R. Collins, W. D. Dover, and D. H. Michael, *Research Techniques in Nondestructive Testing*, R. S. Sharpe, Ed. London, U.K.: Academic, 1985, vol. 8, ch. 5.

[10] A. M. Lewis *et al.*, "Thin-skin electromagnetic fields around surface-breaking cracks in metals," *J. Appl. Phys.*, vol. 64, pp. 3777–3784, 1988.

[11] A. H. Kahn, R. Spal, and A. Feldman, "Eddy-current losses due to a surface crack in conducting material," *J. Appl. Phys.*, vol. 48, pp. 4454–4459, 1977.

[12] J. R. Bowler and N. Harfield, "Evaluation of probe impedance due to thin-skin eddy-current interaction with surface cracks," *IEEE Trans. Magn.*, vol. 34, pp. 515–523, Mar. 1998.

[13] M. Abramowitz and I. A. Stegun, *Handbook of Mathematical Functions with Formulas, Graphs, and Mathematical Tables*. New York: Wiley, 1970.

[14] W. H. Press, B. P. Flannery, S. A. Teukolsky, and W. T. Vetterling, *Numerical Recipes, The Art of Scientific Computing*. Cambridge, MA: CUP, 1988.

[15] D. J. Harrison, L. D. Jones, and S. K. Burke, "Benchmark problems for defect size and shape determination in eddy-current nondestructive evaluation," *J. Nondest. Eval.*, vol. 15, no. 1, pp. 21–34, 1996.

[16] C. V. Dodd and W. E. Deeds, "Analytical solutions to eddy-current probe-coil problems," *J. Appl. Phys.*, vol. 39, pp. 2829–2838, 1968.

[17] M. McIver, "An inverse problem in electromagnetic crack detection," *IMA J. Appl. Math.*, vol. 47, pp. 127–145, 1991.

[18] I. S. Gradshteyn and I. M. Ryzhik, *Tables of Integrals Series and Products*, 4th ed. New York: Academic , 1965.